^{15}N NMR Chemical Shift Tensors of Substituted Hexaazaisowurtzitanes: The Intermediates in the Synthesis of CL-20†

Jacalyn S. Clawson,‡ Karen L. Anderson,§ Ronald J. Pugmire,‡ and David M. Grant*,‡

Department of Chemistry, University of Utah, Salt Lake City, Utah 84112, and ATK Thiokol Propulsion, P.O. Box 707, Brigham City, Utah 84302

Received: November 7, 2003; In Final Form: January 23, 2004

Several cage-substituted hexaazaisowurtzitanes [2,4,6,8,10,12-hexabenzyl-2,4,6,8,10,12-hexaazaisowurtzitane (HBIW); 2,6,8,12-tetraacetyl-4,10-dibenzyl-2,4,6,8,10,12-hexaazaisowurtzitane (TADB); and 2,6,8,12-tetraacetyl-4,10-diformyl-2,4,6,8,10,12-hexaazaisowurtzitane (TADF)] have been synthesized as intermediate steps in the synthesis of CL-20. The ^{15}N NMR isotropic and chemical shift tensor principal values have been obtained for these intermediates using CP/MAS and FIREMAT methods. Solid-state ^{15}N NMR offers unique advantages in the study of these materials, due to solubility issues and lack of high-quality X-ray crystallographic data. In addition, the caged structures possess unique electronic properties that can be useful in further refining theoretical methods. The effects of the different functional groups on the chemical shift tensor principal values of these caged amines have been evaluated and are shown to be reflected in the total anisotropy. The position of the amine within the cage is manifested in the δ_{22} values. Nitrogen-15 NMR shielding calculations using the embedded ion method (EIM) to account for long-range intermolecular interactions show a good correlation, rmsd = 4 ppm, with the observed chemical shift tensor values.

Introduction

Recent developments in the design of new energetic materials have focused on cagelike molecules that have a significantly higher density than their related monocycles and contain strain energy that can be released during detonation. 2,4,6,8,10,12-hexanitro-2,4,6,8,10,12-hexaazaisowurtzitane (HNIW or CL-20) is the most promising of these new explosives.[1] As part of a continued study to relate chemical shift tensor principal values (CST PVs) to the characteristics of explosives, CL-20 has been selected for its large detonation velocity and moderate sensitivity to impact.[2] Several cage-substituted isowurtzitanes are generated as intermediate steps in the synthesis of CL-20 using the ATK Thiokol process: 2,4,6,8,10,12-hexabenzyl-2,4,6,8,10,12-hexaazaisowurtzitane (HBIW), 2,6,8,12-tetraacetyl-4,10-dibenzyl-2,4,6,8,-10,12-hexaazaisowurtzitane (TADB), and 2,6,8,12-tetraacetyl-4,10-diformyl-2,4,6,8,10,12-hexaazaisowurtzitane (TADF) (see Figure 1).[3] For convenience, the isowurtzitane cage will be referred to in two parts: the *attic*, which contains the nitrogens (N1−N4) and bridge carbons of the five-membered rings, and the *basement*, which consists of the six-membered ring. The ^{15}N CST PVs of these intermediates have been measured and correlated with calculated ^{15}N chemical shielding principal values. Substitutent effects on CST PVs of caged amines have been evaluated. The ^{15}N chemical shift tensors of strained unsaturated nitrogen−carbon ring systems such as these have not been previously measured. The study of such systems improves our understanding of the relationship between ^{15}N electronic environment and structure.

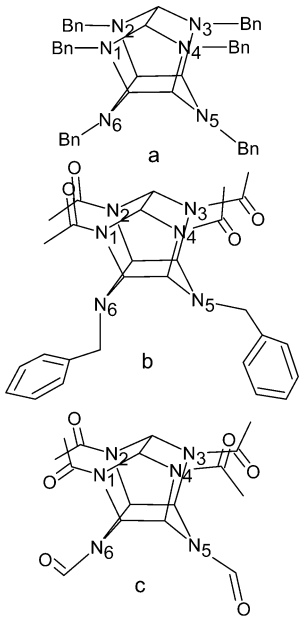

Figure 1. Numbering scheme used in this paper for HBIW (a), TADB (b), and TADF (c). Functional group orientations for TADB and TADF are taken from X-ray data.

Nitrogen-15 electronic environments are quite sensitive to molecular structure and to intermolecular effects.[4] Recent work from this laboratory[5] has shown that reasonable ^{15}N chemical shielding tensors, which are linearly related to the CST, can be calculated in molecules with large charge separations, when long-range crystal interactions are included in the calculations. These interactions are implemented in the calculations using the embedded ion method (EIM).[6] This method is one of several charge models[7] that reproduce the electrostatic potential for a molecule of interest using an array of partial atomic point

† Approved for public release by the Naval Air Warfare Center Weapons Division, 19 Sept 2003.

* To whom correspondence should be addressed. E-mail: grant@chemistry.utah.edu.

‡ University of Utah.

§ ATK Thiokol Propulsion.

10.1021/jp0373999 CCC: $27.50
Published on Web 03/17/2004

charges. This method places the point charges at the crystallographic sites and varies the outermost charges to obtain the correct electrostatic potential. A complete description of the EIM can be found in ref 6.

In addition to the magnitudes of the chemical shielding tensor, the orientation of the tensor in the molecular frame can be calculated with reasonable accuracy.[5,8] This orientational information cannot be obtained experimentally from powder samples. Integrating the directional chemical shielding results with solid-state chemical shift data provides valuable insight into the molecular structure of these caged amines.

Structural information regarding HBIW is of particular interest, since its single crystals are twinned and, thus, a refined X-ray structure cannot be determined. The crystalline structures of TADB[9] and TADF[10] have been determined by X-ray diffraction. Shielding computations on optimized TADB and TADF molecules provided an estimate of the accuracy that is attainable for optimized cage structures. Characterization of HBIW by solid-state NMR provides essential information on its crystal structure, including the number of molecules per asymmetric unit. A proposed structure of HBIW has been determined from chemical shielding calculations on optimized structures of HBIW.

Experimental Section

Materials. The experiments were carried out on 95% ^{15}N-enriched intermediates provided by ATK Thiokol Propulsion. TADB and TADF samples were verified by X-ray powder diffraction; experimental diffraction patterns were compared to calculated patterns made from the single-crystal structure using the Insight II program.[11] All intermediates were verified by ^{1}H solution-state NMR spectroscopy.

Acquisition of NMR Data. Spectra were collected on a CMX400 NMR spectrometer operating at 400.12 MHz for ^{1}H and 40.55 MHz for ^{15}N. All spectra were externally referenced to ^{15}N-glycine at −347.5 ppm on the nitromethane scale.[12] CP/MAS spectra were collected at a spinning rate of 4 kHz. Cross-polarization was achieved with contact times of 2.0, 3.0, and 4.5 ms for HBIW, TADB, and TADF, respectively. Saturation recovery experiments were used to determine the proton T_1 of each intermediate as follows: 3, 12, and 5 s for HBIW, TADB and TADF, respectively. Pulse delays were multiples of the T_1 determined from constant time experiments. Nitrogen-15 chemical shift principal values were measured from FIREMAT[13] experiments. Continuous wave (CW) ^{1}H decoupling was used in all three FIREMAT experiments. The following FIREMAT parameters were used: *HBIW*. The $\pi/2$ ^{1}H pulse width of 5.2 μs was used with a ^{15}N π pulse width of 14.0 μs. Evolution and acquisition dimension spectral widths were 16.2 and 2.7 kHz, respectively. A total of 16 evolution increments of 288 scans each were collected. A spinning speed of 169 Hz was used. *TADB*. The $\pi/2$ ^{1}H pulse width of 5.2 μs was used with a ^{15}N π pulse width of 14.0 μs. Spectral widths of 30.2 and 5.0 kHz were used for the evolution and acquisition dimensions, respectively. A total of 16 evolution increments of 96 scans each were collected. A spinning speed of 315 Hz was used. *TADF*. The $\pi/2$ ^{1}H pulse width of 4.0 μs was used with a ^{15}N π pulse width of 11.0 μs. Spectral widths of 63.4 and 10.6 kHz were used for the evolution and acquisition dimensions, respectively. A total of 16 evolution increments of 192 scans each were collected. A spinning speed of 660 Hz was used.

Methods

Calculations. All quantum calculations were performed with the *Gaussian 98* package.[14] Geometry optimizations were performed using Hartree−Fock (HF) theory[15] and the 6-311G basis set.[16] Even at the HF level, full geometry optimizations of the isowurtzitane intermediates required significant computational time, ranging from one to three weeks; thus, higher levels of theory were not explored. Proton optimizations were carried out on the X-ray crystal structures of TADB[9] and TADF[10] prior to calculating shielding tensors on the isolated molecules. Full geometry optimizations were also performed on isolated molecules of all three intermediates. When an X-ray crystal structure was available, the EIM[6] was used to incorporate intermolecular interactions into the model. Natural bond order (NBO)[17] charges calculated with the B3LYP/D95**[18] level of theory were used for the partial atomic charges in the EIM. Work from this lab[19] has shown that the choice of charge model has little or no effect on the calculated chemical shielding values. Chemical shielding tensors were computed using the gauge-invariant atomic orbital (GIAO) method[20] employing the B3LYP/6-311+G**[16] level of theory. The ^{15}N chemical shielding principal values were converted to chemical shifts by a best fit line to the experimental data. The intercept should be the absolute shielding value of nitromethane, −135.8 ppm.[21] Shielding and shift are inversely proportional, so the slope should be −1. Deviations from this value are indicative of the error introduced by the method and the basis set.[22]

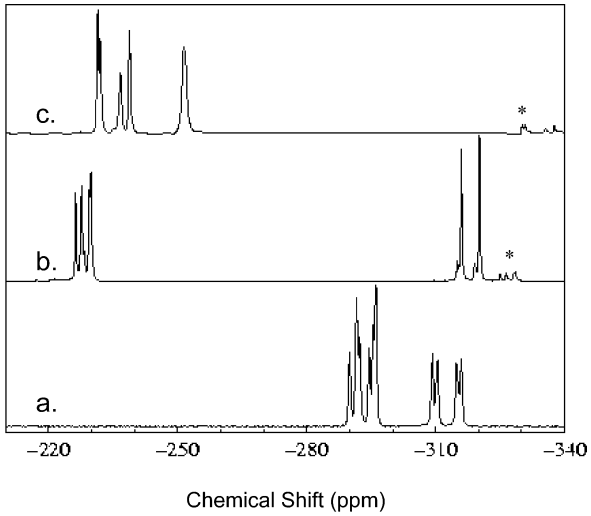

Figure 2. ^{15}N CP/MAS spectra at 4 kHz of the CL-20 intermediates studied: (a, bottom) HBIW; (b, center) TADB; (c, top) TADF. Spinning sidebands are indicated with asterisks.

Results

Spectral Assignments. Figure 2 presents the ^{15}N CP/MAS spectra of the three CL-20 intermediates measured, and Figure 3 presents the ^{15}N FIREMAT of TADB. The signal-to-noise ratios of the FIREMAT spectra of HBIW and TADF are comparable. A complete list of all measured tensors is included in Figure 1 of the Supporting Information. The assigned experimental ^{15}N CST PVs obtained from FIREMAT data are summarized in Table 1. Tables 2−4 summarize the calculated chemical shift principal values employing several molecular models: isolated molecule using X-ray geometry, EIM, and optimized molecule. Peak assignments were based on minimization of the root-mean-square distance (rmsd) between experimental and calculated CST PVs (see Table 1). *F*-tests established the probabilities of the rmsd-minimum assignment relative to other possibilities.

HBIW. Ten magnetically nonequivalent nitrogen resonances were measured for HBIW. The nitrogen resonances at −291.6

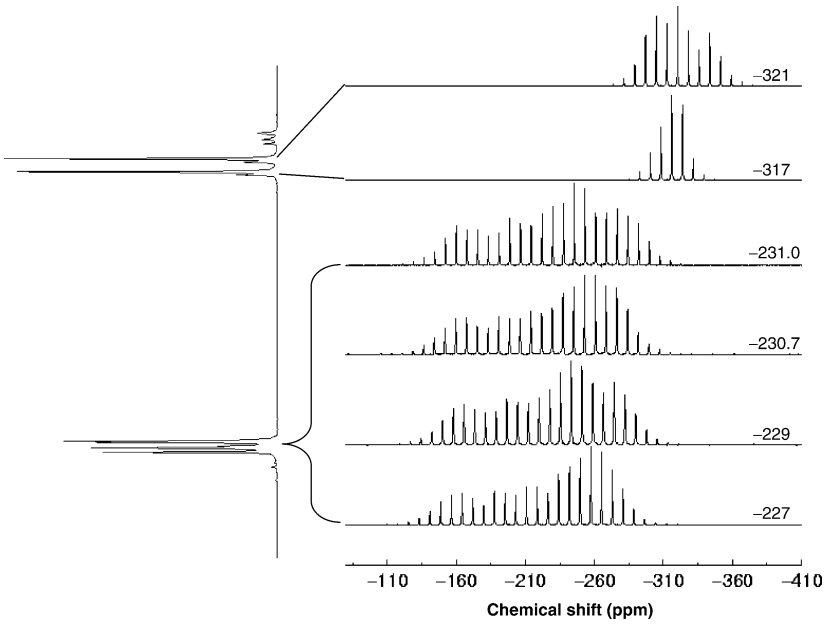

Figure 3. ^{15}N FIREMAT spectrum of TADB.

TABLE 1: Summary of Experimental ^{15}N Chemical Shift Principal Values of the CL-20 Intermediates[a]

compd[b]	assignment	δ_{iso} ppm	δ_{11} ppm	δ_{22} ppm	δ_{33} ppm	span[c]	no. of CST avg[d]
HBIW[e]	N1 and N3	−297	−272	−294	−324	52	3[g]
	N2 and N4	−292	−262	−285	−331	69	3[g]
	N5 or N6[f]	−317	−292	−321	−337	45	2
	N6 or N5[f]	−311	−285	−318	−330	45	2
TADB	N1	−231	−140	−245	−308	167	
	N2	−229	−140	−248	−299	159	
	N3	−227	−136	−256	−290	154	
	N4	−231[h]	−139	−256	−297	158	
	N5	−317	−295	−320	−336	40	
	N6	−321	−286	−317	−361	76	
TADF	N1	−238	−149	−256	−308	159	
	N2 and N4	−233	−146	−249	−304	158	2
	N3	−240	−154	−257	−309	154	
	N5 and N6	−253	−141	−297	−320	179	2

[a] See Figure 1 of the Supporting Information for a complete list of the experimental CST PVs. [b] See Figure 1 for structure and numbering scheme. [c] Span = δ_{11} − δ_{33}. [d] Number of experimental CST PVs averaged. If blank, only one tensor was measured. [e] HBIW has two molecules per asymmetric unit. [f] Assignment could not be determined by comparison to calculated shieldings. Unlike the averaged assignments, these experimental tensors were significantly different and, thus, were not averaged. [g] The three tensors account for four nitrogen atoms. One resonance had twice the intensity of the other two. [h] The peak was separated from N1 resonance by 0.3 ppm.

and −296.2 ppm have approximately twice the area of the remaining eight peaks, giving a total of 12 nitrogens in the HBIW crystal. The presence of two isotropic lines per nitrogen in HBIW suggests that the HBIW crystal has two molecules per asymmetric unit. Prabhakaran et al.[23] measured the ^{15}N chemical shifts of HBIW in acetone-d_6, assigning the 2:1 resonances at −295.9 and −316.1 ppm to the attic and basement amines, respectively. Correspondingly, the six CP/MAS peaks centered around −292 ppm have been assigned to the attic nitrogen atoms and the two pairs near −311 and −317 ppm have been assigned to the basement amines.

Since no reliable X-ray crystal structure exists, shielding calculations were carried out on fully optimized HBIW molecules. There are several derivatives of HBIW with substituents on the benzyl group, including chloro, methyl, bromo, fluoro, and methoxy groups.[2] The derivatives have similar cage structures differing in the orientation of the benzyl groups. Unfortunately, none of the crystal structures of the derivatives have two molecules per asymmetric unit, as is the case for the HBIW crystal. There are essentially two structures, one in which all of the attic groups are pointing up, as in the methoxy derivative,[2] and one in which the attic groups are pointing up and down, as is the case for the chloro derivative.[24] Thus, two HBIW structures with these two different starting geometries were generated and optimized. Figure 4 shows the two derivatives and the two optimized HBIW molecules. Optimization

TABLE 2: Calculated ^{15}N CST PVs on Single Molecules Using X-ray Geometry

compd	assignment	δ_{iso}^{calcd} ppm	δ_{11}^{calcd} ppm	δ_{22}^{calcd} ppm	δ_{33}^{calcd} ppm
TADB	N1	−238	−154	−243	−316
	N2	−233	−148	−247	−305
	N3	−232	−137	−260	−298
	N4	−235	−140	−264	−300
	N5	−316	−291	−323	−333
	N6	−322	−286	−317	−363
TADF	N1	−235	−153	−248	−306
	N2 and N4	−231	−148	−239	−307
	N3	−236	−153	−247	−309
	N5 or N6	−250	−134	−304	−312
	N6 or N5	−244	−124	−295	−313
slope	−1.01 ± 0.02	intercept	−143 ± 4	rmsd	7 ppm

TABLE 3: Calculated ^{15}N CST PVs Using the EIM

compd	assignment	δ_{iso}^{calcd} ppm	δ_{11}^{calcd} ppm	δ_{22}^{calcd} ppm	δ_{33}^{calcd} ppm
TADB	N1	−230	−143	−244	−304
	N2	−231	−144	−247	−301
	N3	−229	−137	−254	−295
	N4	−232	−139	−262	−297
	N5	−316	−289	−321	−337
	N6	−322	−286	−317	−362
TADF	N1	−237	−150	−257	−306
	N2 and N4	−234	−146	−249	−305
	N3	−242	−157	−257	−312
	N5 or N6	−253	−139	−305	−316
	N5 or N6	−251	−136	−298	−319
slope	−1.048 ± 0.007	intercept	−159 ± 2	rmsd	4 ppm

TABLE 4: Calculated ^{15}N CST PVs on Optimized Single Molecules

		δ_{iso}^{calcd}	δ_{11}^{calcd}	δ_{22}^{calcd}	δ_{33}^{calcd}
compd	assignment	ppm	ppm	ppm	ppm
HBIW	N1 and N3	−297	−270	−290	−331
	N2 and N4	−291	−254	−285	−334
	N5 and N6	−312	−289	−316	−334
TADB	N1	−235	−147	−250	−309
	N2	−233	−149	−248	−304
	N3	−232	−138	−261	−297
	N4	−233	−141	−258	−300
	N5	−319	−296	−323	−339
	N6	−319	−285	−315	−358
TADF	N1	−242	−155	−260	−310
	N2 and N4	−237	−151	−241	−317
	N3	−242	−155	−259	−310
	N5 and N6[a]	−247	−127	−300	−315
slope	−1.02 ± 0.01	intercept	−155 ± 3	rmsd	5 ppm

[a] The formyl groups became identical during optimization; therefore, the shielding tensor principal values were averaged.

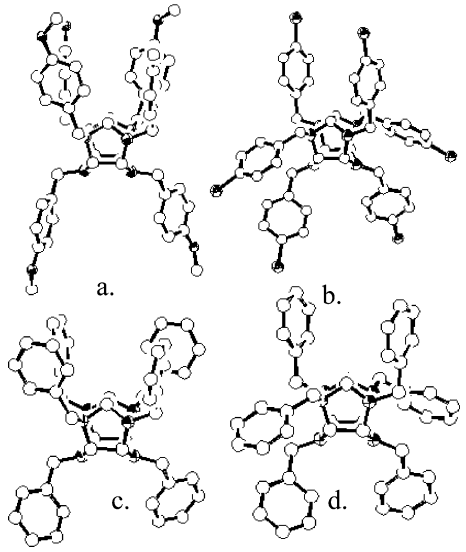

Figure 4. Optimized structures of HBIW using the HF/6-311G level of theory: (a) MeOH−HBIW X-ray structure before MeOH was replaced by H and optimized; (b) Cl−HBIW X-ray structure before Cl was replaced by H and optimized; (c) optimized methoxy-derived HBIW structure; (d) partially optimized chloro-derived HBIW structure. Note: the shaded N atoms are easily recognized from Figure 1.

altered the bond lengths and angles a negligible amount: ±0.01 Å and ±5°, respectively. The orientations of the benzyl groups are defined by two of the torsional angles. The bend of the CH_2-C bond off *or* away from the cage is defined by the CH−N−CH_2−C angle, and the N−CH_2−C−CH angle defines the twist in the benzene ring. The two torsion angles are given in Table 5 for each molecule before and after optimization. The torsion angles of TADB and TADF are also provided for comparison. As one can see, the torsion angles have changed during optimization. This seemingly large change was also observed when the TADB molecule was optimized, but it had little effect on the calculation of the benzylamines' principal shielding values. One would expect both starting geometries to optimize to a single energy-minimized structure. Since this was not the case, the energies of the two optimized structures were examined. The structures differ in energy by 3 kcal/mol, which is greater than the error of 0.6 kcal/mol estimated from the vibrational energy at 25 °C. However, it is not outside the range of energy differences observed between polymorphs. For example, using the same level of theory single-molecule

TABLE 5: Torsion Angles in Degrees of the Functional Groups of the Isowurtzitane Cage

compd	torsion angle[a]	N1	N2	N3	N4	N5	N6
	Benzyl Groups						
MeOH−HBIW	CH−N−CH_2−C	71	64	63	63	150	145
	N−CH_2−C−CH	75	81	62	75	118	97
methoxy-derived	CH−N−CH_2−C	78	65	78	65	152	152
HBIW	N−CH_2−C−CH	75	67	75	67	138	138
Cl−HBIW	CH−N−CH_2−C	179	47	179	47	148	148
	N−CH_2−C−CH	123	55	123	55	155	155
chloro-derived	CH−N−CH_2−C	172	59	167	59	141	60
HBIW	N−CH_2−C−CH	118	61	120	60	134	43
TADB	CH−N−CH_2−C		see below			151	63
	N−CH_2−C−CH					126	77
	Acetyl and Formyl Groups						
TADB	CH−N−C=O	4	182	7	181	see above	
TADF	CH−N−C=O	190	185	6	4		

[a] See Figure 5.

calculations, ϵ and γ CL-20 show an energy difference of 6 kcal/mol. Therefore, we cannot eliminate either HBIW structure on the basis of energy considerations alone.

NMR shielding calculations were performed on both optimized structures. Since the basement groups of the chloro-derived HBIW changed so dramatically, with both benzyl groups facing the same direction, calculations were also performed on a molecule in which the basement torsion angles were not optimized. Each of the optimized structures' principal shielding components was correlated to the experimental CST PVs. Agreement using the methoxy-derived structure was significantly better than that with either the optimized or partially optimized chloro-derived structures. For example, the rmsd's of the correlations were 4 and 8 ppm between the fully optimized methoxy- and chloro-derived structures, respectively. Thus, NMR predicts that both molecules of HBIW resemble the methoxy derivative structure. The 4 ppm error is comparable to that for the correlation using optimized isolated molecules of TADF and TADB, where the rmsd was 6 ppm. Not only is the error of HBIW comparable, for optimized structures correlation errors are similar to the results using X-ray structures (see Tables 2 and 4). However, the intercept of the correlation plot using optimized TADF and TADB structures was significantly different than the X-ray correlated intercept, −155 ± 3 and −143 ± 4 ppm, respectively.

Only six chemical shielding tensors are available from the lowest-rmsd optimized HBIW calculation. Therefore, the two molecules in the asymmetric unit could not be identified. To assign the tensors, the experimental tensors corresponding to the attic amines were separated into two groups and averaged. The maximum standard deviation within the two sets of attic amine principal values was ±3 ppm. The averaging of the tensors suggests that the two molecules in the HBIW crystal have similar structures. Consequent assignment shows that the attic amine can be categorized by the orientation of the benzyl groups. The −297 ppm CSTs are assigned to N1 and N3 with the torsion angles CH−N−CH_2−C = 78° and N−CH_2−C−CH = 75°, and the −292 ppm CSTs are assigned to N2 and N4 with the torsion angles CH−N−CH_2−C = 65° and N−CH_2−C−CH = 67° (see Tables 1 and 5 and Figure 5). Similar experimental CST PVs of basement amines were also averaged. Experimentally, the basement benzylamines differ in their δ_{11} components of −285 or −292 ppm. Theory was unable to distinguish between the two basement tensors, since the benzyl groups are identical in the hypothesized isolated optimized structure.

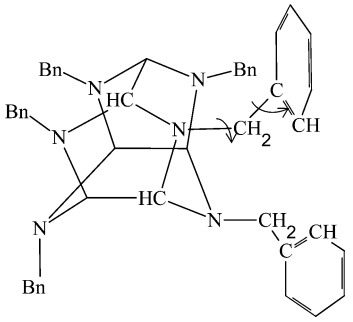

Figure 5. Torsion angles of the benzyl groups in HBIW.

TADB and TADF. Tables 2 and 3 show the calculated chemical shift principal values using the isolated molecule method and the EIM, respectively, including the best-fit regression line for each correlation. The exceptionally good error (rmsd = 7 ppm) found by only the isolated molecules is not surprising, considering the positioning of the amine within the interior of the structure and the lack of nearest neighbor interactions, such as hydrogen bonding. Despite this, there is still a 43% reduction in the error using the EIM, indicating that significantly long-range electrostatic interactions do occur within the crystal. This improvement in theory illustrates the extreme sensitivity of the ^{15}N chemical shift tensor to the surrounding crystal and the need to include such interactions in ^{15}N shielding calculations. The following peak assignments and *F*-test percentages are based on calculated EIM shielding tensors.

TADB. The peaks located near −230 and −319 ppm in TADB spectrum are clearly separated and may be assigned to acetyl-substituted and benzyl-substituted amines, respectively. The two benzyl-substituted nitrogens have significantly different tensors; thus, their assignment based on calculated values is unequivocal. Acetyl-substituted amines can be easily separated by the orientation of the carbonyl oxygen to the basement: N1/N2, where the carbonyl oxygens are pointing up, and N3/N4, where the carbonyl oxygens are pointing down. These groups are clearly assignable by theory. However, assignment within the pairs is not so clear. There is only 78% confidence that the peaks at −231.0 ppm (N1) and −229 ppm (N2) are correctly assigned, whereas N3 and N4 are assigned with higher confidence (*F*-test: 92%). Note that, despite their near isotropic degeneracy, the peaks at −230.7 and −231.0 ppm are assigned to different amines, further demonstrating the value in measuring the CST PVs.

TADF. Assignment of peaks in TADF spectrum is similar to that for TADB; the formyl- and acetyl-substituted amines are sufficiently separated spectroscopically, and assignment by type is straightforward. The acetyl amine can be easily separated by carbonyl orientation. N1 and N3 tensors are classified by their δ_{11} values and have been assigned. However, the principal components of the −232.5 and −233.2 ppm peaks (N2 and N4) are too similar to make a distinction. The formyl amines (N5 and N6) also cannot be distinguished due to the similarity of their CST PVs. The indistinguishable tensors have been averaged in Table 1.

Discussion

There are several notable observations that emerge from the chemical shift principal values measured here. The change in isotropic shift of the basement and the attic benzyl-substituted amines is due solely to the δ_{11} and δ_{22} components. The liquid-state isotropic data exhibited a large separation between the attic and basement amines but no separation within the two groups.

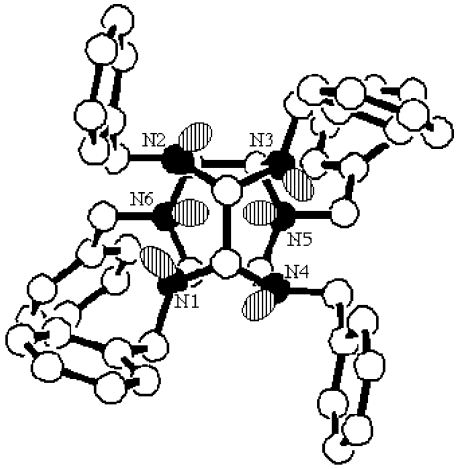

Figure 6. Orientation of the nitrogen lone pairs, shown in gray, for the rmsd-minimized structure of HBIW.

In the solid-state there are significant differences in the entire chemical shift tensors of the attic amines. The variation in benzyl-substituted amines may be attributed to several possible factors: additional ring strain on the five-membered rings, orientation of the lone pair on the nitrogen, or orientation of the functional group with respect to the cage. The orientations of the functional groups are summarized in Table 5 and have been the basis of many of the assignments. In the attic, the nitrogen lone pairs face away from each other, facing either the seven- or five-membered rings. Nitrogen lone pairs in the basement point toward each other and the six-membered ring (see Figure 6). The profound effect that large changes in the orientations of the benzyl group and the lone pair have on the CST PVs is illustrated by the basement benzylamines, N5 and N6, of TADB (see Table 1). The axial orientation of N6 is reflected in a significant (∼30 ppm) increase in the δ_{33} principal values as compared to those for the equatorial orientation of N5. In addition, the calculated orientations of the PVs with respect to the molecular frame are significantly different for equatorially and axially oriented benzylamines. The orientations of the TADB PVs are not given explicitly, since the amine is sp^3 hybridized and components are not perpendicular to a bond or lone pair; thus, no direct correlation between shielding component and structure can be made. The experimental δ_{33} values of HBIW basement amines are consistent with the equatorial amine in TADB, suggesting that the orientations of basement benzyl groups in HBIW are approximately equatorial.

As expected, the largest change in the amine's electronic environment is seen when HBIW is converted to TADB, with changes of ∼100 ppm in the isotropic shift and a significant increase in span. This is a result of the four attic benzyl groups being replaced with acetyl groups. When a carbonyl is placed next to a nitrogen, several resonance structures contribute to the electronic environment, which is reflected structurally by the shortening of the N−CO bond from 1.45 to 1.35 Å and the flattening of the C_1C_2N(cage)C=O into a planelike geometry. Thus, the amine is essentially sp^2 hybridized. The direction in which the oxygen of the carbonyl group points relative to the basement is reflected in the δ_{22} value of the acetylamine. The acetylamine δ_{22} is −256 ppm when the oxygen is pointing down toward the basement and −246 ppm when it is pointing up (see Figure 1). As shown in Figure 7, theoretical calculations place the σ_{22} out of the plane and 75° above the N−CO bond; therefore, most of the contribution to the experimental δ_{22} is coming from the σ bond. The N−C(carbonyl) bond lengths of TADB and TADF are all equivalent. Thus, there is no chemical

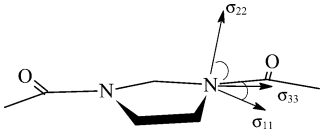

Figure 7. Orientation of the acetylamine CST PVs to the molecular frame. The five-membered ring has been separated from the isowurtzitane cage for simplicity.

TABLE 6: Calculated ^{15}N CST PVs of HFIW

compd	assignment[a]	$\delta_{iso}^{calcd\ b}$ ppm	$\delta_{11}^{calcd\ b}$ ppm	$\delta_{22}^{calcd\ b}$ ppm	$\delta_{33}^{calcd\ b}$ ppm	span
HFIW	N1	−225	−124	−250	−300	176
	N2	−221	−128	−238	−298	170
	N3	−227	−127	−251	−301	174
	N4	−222	−127	−241	−298	171
	N5	−248	−133	−296	−314	181
	N6	−243	−124	−291	−314	190

[a] The numbering scheme and functional group orientations are identical to those for TADF. [b] Chemical shifts were calculated using the TADB and TADF isolated molecule correlation line of $\delta^{calcd} = (\sigma^{calcd} + 143)/-1.01$.

information to explain why the orientation of the carbonyl to the basement would affect the N−C σ bond and, accordingly, the chemical shift component perpendicular to it.

Exchanging formyl groups for the benzyls in the basement seems to affect the acetylamine CST. The δ_{11} values of the acetylamines in TADB are downfield by ∼10 ppm from the TADF values. This may reflect a long-range substitutent effect or steric effects on the structure. The δ_{11} component, which is 75° from the π orbitals of the N−C bond (see Figure 7), reflects the amount of π-electron resonance. The increase in δ_{11} indicates that the TADF acetyl groups experience a greater contribution from the N=CO$^-$ resonance structure.

Compared to acetylamine CST PVs, the CST PVs of formyl-substituted amines in TADF show a small increase in span ($\delta_{11} - \delta_{33}$) and a significant (40 ppm) upfield shift in the δ_{22} value. It is unlikely that substituting a proton for the methyl group would have a significant effect on the π-electron structure. These changes could come from several sources, including attic or basement positioning of the amine. To help determine the source of the difference between the formyl and acetyl CSTs, shielding tensors were calculated on 2,4,6,8,10,12-hexaformyl-2,4,6,8,10,12-hexaazaisowurtzitane (HFIW) (see Table 6). The single molecule of HFIW was generated using the TADF X-ray structure with the methyl of the acetyl groups replaced by a hydrogen atom. As Table 6 clearly shows, the change in δ_{22} of the formylamine is due to the functional group positioning in the cage rather than substitutent effects. This is the same affect on δ_{22} observed for the attic and basement benzyl-substituted amines in HBIW.

Conclusions

The amine chemical shift tensors in substituted isowurtzitane cages have been described, and the power of connecting data to calculated chemical shielding values has been demonstrated. The data show that amine CST PVs in strained cages are sensitive to the type of substitutent, the orientation of the substitutent, and placement of the substitutent in the cage. Regardless of the substitutents attached to the cage, the amine CST PVs are affected by intermolecular interactions. Acetyl- and formyl-substituted amines have equivalent electronic environments. However, benzyl-substituted amines and acetyl/formyl-substituted amines have unrelated electronic environments. For all functional groups the basement/attic positioning of the amine within the isowurtzitane cage influences the δ_{22} principal value. From chemical shielding calculations, further insight into the crystal structure of HBIW has been gained. Both HBIW molecules in the asymmetric unit have attic benzyl groups that point up and basement benzyl groups in the equatorial conformation. The results also suggest that the attic benzyl groups have different torsion angles. This work further demonstrates the value of the EIM in obtaining accurate nitrogen chemical shielding tensors in molecules with large charge separation, even in the absence of nearest neighbor interactions.

Acknowledgment. Computer resources for the tensor computations were provided by the Center for High Performance Computation at the University of Utah. This work was supported by the Department of Energy under Grant DE-FG03-94ER-14452 and by ATK Thiokol Internal Research and Development (IR&D) funding. The labeled compounds were available from the Strategic Environmental Research and Development Program (SERDP). We would like to acknowledge the contributions of the late Thomas K. Highsmith in the syntheses of these compounds.

Supporting Information Available: Figures containing the ^{15}N chemical shift principal values for all the CL-20 intermediates measured in this study and the structures of the three CL-20 intermediates. This material is available free of charge via the Internet at http://pubs.acs.org.

References and Notes

(1) Nielsen, A. T.; Nissan, R. A.; Vanderah, D. J.; Coon, C. L.; Gilardi, R. D.; George, C. F.; Flippen-Anderson, J. *J. Org. Chem.* **1990**, *55*, 1459.

(2) Simpson, R. L.; Urtiew, P. A.; Ornellas, D. L.; Moody, G. L.; Scribner, K. J.; Hoffman, D. M. *Propellants, Explos., Pyrotech.* **1997**, *22*, 249.

(3) Wardle, R. B.; Edwards, W. W. U.S. Patent 5,739,325, 1988.

(4) Witanowski, M.; Stefaniak, L.; Webb, G. A. In *Annual Reports on NMR Spectroscopy*; Webb, G. A., Ed.; Academic Press: New York, 1981; Vol. 11B.

(5) Clawson, J. S.; Strohmeier, M.; Stueber, D.; Orendt, A. M.; Barich, D. H.; Asay, B.; Hiskey, M. A.; Pugmire, R. J.; Grant, D. M. *J. Phys. Chem. A* **2002**, *106*, 6352.

(6) (a) Stueber, D.; Guenneau, F. N.; Grant, D. M. *J. Chem. Phys.* **2001**, *114*, 9236. (b) Stueber, D.; Grant, D. M. *J. Am. Chem. Soc.* **2002**, *124*, 10539.

(7) (a) de Dios, A. C.; Oldfield, E. *Chem. Phys. Lett.* **1993**, *205*, 108. (b) Klintenberg, M.; Derenzo, S. E.; Weber, M. J. *J. Comput. Phys. Commun.* **2000**, *131*, 120.

(8) Solum, M. S.; Altmann, K. L.; Strohmeier, M.; Berges, D. A.; Zhang, Y.; Facelli, J. C.; Pugmire, R. J.; Grant, D. M. *J. Am. Chem. Soc.* **1997**, *119*, 9804.

(9) Nielsen, A. T.; Chafin, A. P.; Christian, S. L.; Moore, D. W.; Nadler, M. P.; Nissan, R. A.; Vanderah, D. J.; Gilardi, R.; George, C. F.; Flippen-Anderson, J. L. *Tetrahedron* **1998**, *54*, 11793.

(10) Gilardi, R. Naval Research Laboratory, Washington, DC, unpublished results.

(11) *Insight II*, version 4.0.0P+; Accelrys, Inc.: San Diego, CA, 2000.

(12) Measured value using a cylindrical sample of 99% ^{15}N labeled nitromethane.

(13) Alderman, D. W.; McGeorge, G.; Hu, J. Z.; Pugmire, R. J.; Grant, D. M. *Mol. Phys.* **1998**, *95*, 1113.

(14) Frisch, M. J.; Trucks, G. W.; Schlegel, H. B.; Scuseria, G. E.; Robb, M. A.; Cheeseman, J. R.; Zakrzewski, V. G.; Montgomery, J. A., Jr.; Stratmann, R. E.; Burant, J. C.; Dapprich, S.; Millam, J. M.; Daniels, A. D.; Kudin, K. N.; Strain, M. C.; Farkas, O.; Tomasi, J.; Barone, V.; Cossi, M.; Cammi, R.; Mennucci, B.; Pomelli, C.; Adamo, C.; Clifford, S.; Ochterski, J.; Petersson, G. A.; Ayala, P. Y.; Cui, Q.; Morokuma, K.; Salvador, P.; Dannenberg, J. J.; Malick, D. K.; Rabuck, A. D.; Raghavachari, K.; Foresman, J. B.; Cioslowski, J.; Ortiz, J. V.; Baboul, A. G.; Stefanov, B. B.; Liu, G.; Liashenko, A.; Piskorz, P.; Komaromi, I.; Gomperts, R.; Martin, R. L.; Fox, D. J.; Keith, T.; Al-Laham, M. A.; Peng, C. Y.; Nanayakkara, A.; Challacombe, M.; Gill, P. M. W.; Johnson, B.; Chen,

W.; Wong, M. W.; Andres, J. L.; Gonzalez, C.; Head-Gordon, M.; Replogle, E. S.; Pople, J. A. *Gaussian 98*, revision A.11; Gaussian, Inc.: Pittsburgh, PA, 2001.

(15) (a) Roothan, C. C. *J. Mod. Phys.* **1951**, *23*, 69. (b) Pople, J. A.; Nesbet, R. K. *J. Chem. Phys.* **1954**, *22*, 571. (c) McWeeny, R.; Dierksen, G. *J. Chem. Phys.* **1968**, *49*, 4852.

(16) (a) McLean, A. D.; Chandler, G. S. *J. Chem. Phys.* **1980**, *72*, 5639. (b) Krishnan, R.; Binkley, J. S.; Seeger, R.; Pople, J. A. *J. Chem. Phys.* **1980**, *72*, 650.

(17) (a) Glendening, E. D.; Reed, A. E.; Carpenter, J. E.; Weinhold, F. *NBO*, version 3.1. (b) Carpenter, J. E.; Weinhold, F. *THEOCHEM* **1988**, *169*, 41. (c) Carpenter, J. E. Ph.D. Thesis, University of Wisconsin, 1987. (d) Foster, J. P.; Weinhold, F. *J. Am. Chem. Soc.* **1980**, *102*, 7211. (e) Reed, A. E.; Weinhold, F. *J. Chem. Phys.* **1983**, *78*, 4066. (f) Reed, A. E.; Weinhold, F. *J. Chem. Phys.* **1985**, *83*, 1736. (g) Reed, A. E.; Weinstock, R. B.; Weinhold, F. *J. Chem. Phys.* **1985**, *83*, 735. (h) Reed, A. E.; Curtiss, L. A.; Weinhold, F. *Chem. Rev.* **1988**, *88*, 899. (i) Weinhold, F.; Carpenter, J. E. *The Structure of Small Molecules and Ions*; Plenum Publishing: New York, 1988; p 227.

(18) (a) Becke, A. D. *J. Chem. Phys.* **1993**, *98*, 5648. (b) Pople, J. A.; Head-Gordon, M.; Fox, D. J.; Raghavachari, K.; Curtiss, L. A. *J. Chem. Phys.* **1989**, *90*, 5622. (c) Curtiss, L. A.; Jones, C.; Trucks, G. W.; Raghavachari, K.; Pople, J. A. *J. Chem. Phys.* **1990**, *93*, 2537. (d) Dunning, T. H., Jr.; Hay, P. J. In *Modern Theoretical Chemistry*; Schaefer, H. F., III., Ed.; Plenum Publishing: New York, 1976; pp 1−28.

(19) (a) Clawson, J. S. Unpublished results. (b) Strohmeier, M.; Stueber, D.; Grant, D. M. *J. Phys. Chem. A* **2003**, *107*, 7629.

(20) (a) Wolinski, K.; Hilton, J. F.; Pulay, P. *J. Am. Chem. Soc.* **1990**, *112*, 8251. (b) Dodds, J. L.; McWeeny, R.; Sadlej, A. J. *Mol. Phys.* **1980**, *41*, 1419. (c) Ditchfield, R. *Mol. Phys.* **1974**, *27*, 789. (d) McWeeny, R. *Phys. Rev.* **1962**, *126*, 1028. (e) London, F. *J. Phys. Radium* **1937**, *8*, 397.

(21) Jameson, C. J.; Jameson, A. K.; Oppusunggu, D.; Wille, S.; Burrell, M.; Mason, J. *J. Chem. Phys*. **1981**, *74* (1), 81.

(22) Pearson, J. G.; Le, H.; Sanders, L. K.; Godbout, N.; Havlin, R. H.; Oldfield, E. *J. Am. Chem. Soc*. **1997**, *119*, 11941.

(23) Parbhakaran, P. V.; George, B. K.; Ravindran, P. V.; Venkatachalam, S.; Kannan, K. G.; Ninan, K. N. 33rd International Annual Conference on ICT, Karlsruhe, Germany, 2002; Vol. 66, p 1.

(24) Crampton, M. R.; Hamid, J.; Millar, R.; Ferguson, G. *J. Chem. Soc., Perkin Trans. 2* **1993**, 923.